

Original Article

Human Gender Prediction Based on Deep Transfer Learning from Panoramic Radiograph Images

Isa Atas

Computer Technology Department, Diyarbakır Vocational School of Technical Sciences, Dicle University, Diyarbakır, 21100, Turkey

Corresponding Author: Isa Atas

E-mail: isa_atas@dicle.edu.tr

Tel: +90 412 2411000 - 7765

Fax: +90 412 2411029

Conflict of interest

There are no conflicts of interest.

Financial Support

None.

Human Gender Prediction Based on Deep Transfer Learning from Panoramic Radiograph Images

Abstract

Background: Panoramic Dental Radiography (PDR) image processing is one of the most widely used methods for gender determination in forensic medicine. Deep learning models are widely used in automated analysis of radiological images today due to their high processing speed, accuracy and stability. A few approach using transfer learning is proposed to gender-classify PDR images.

Methods: In this study, DenseNet121 convolutional neural network (CNN) classifier, which is one of the pre-trained Deep learning architectures, was used. The proposed DenseNet121 network has been expanded and fine-tuned with several additional layers before the final layer to increase its ability to understand more complex patterns from data. At the end of this stage, it has been trained with the dental dataset containing PDR images and has become more experienced. K-fold cross validation method is adopted to increase the accuracy of the proposed DenseNet121 model.

Results: In this study the best performance was achieved for the 4,800 test datasets with a classification accuracy of 97.25%. The proposed model, along with Grad-CAM based analysis also revealed that the mandible circumference and teeth are the most significant areas to consider in gender classification.

Conclusions: It is thought that the results obtained from this study, which was carried out in a wide age range, will contribute to PDR image interpretation in dental biometric information-based human identification systems and are promising for future studies.

Keywords: deep convolutional neural network, transfer learning, gender prediction, fine-tune, panoramic dental radiograph.

Introduction

Nowadays, artificial intelligence is actively used in a variety of domains, particularly in agriculture,^[1,2] health,^[3-6] industry,^[7-9] natural language processing and voice recognition,^[10-12] security,^[13-15] generative networks,^[16,17] remote sensing and hyperspectral imaging^[18-20] etc. However, the modern methods developing rapidly in artificial intelligence technologies have shown remarkable success in image analysis and become more effective in medical applications. This study is based on the ground of the convolutional neural network, which has provided successful results in various image analyses with modern methods. Our dataset consists of 24,000 PDR images acquired from the local patients.

In the events where a significant number of mortalities occur as a consequence of natural disasters or catastrophes, making identification on human residue is necessary through the participation of professionals from various occupational groups. Due to the exposure of human remains to extreme and destructive external forces and their biological decomposition, making such identifications based on the existing remains becomes a challenging process.^[21] The 2014 INTERPOL Disaster Victim Identification Standards emphasizes that DNA analysis, friction ridge analysis, and forensic odontology methods are the primary, most reliable, and efficacious identification techniques.^[22] The determination of biological gender is the initial stage in the identification process.

Gender identification from human skeletal remains has been identified as an important factor in forensic science and bio-archaeology.^[23] When determining gender in the defined areas, it is necessary to use as many methods or features as possible instead of using a single morphological feature as a reference.^[24] In the literature, studies have been carried out for sex prediction with all existing bones of the human skeleton mandible,^[25] calcaneus,^[26] femur,^[24] patella,^[27] occipital condyle,^[28] hand bones^[29] and sternum^[30] are used to predict gender.^[31]

Despite the adversities, the mandible, which is usually known as the strongest, largest, and most resistant bone that remains intact, plays a significant role in gender prediction in forensic odontology.^[32] Therefore, the mandible, a skeletal component, is the focus.

Rather than taking a single morphological character as a reference, it is necessary to use as many procedures or features as possible while determining the gender of the unknown skeletal residues.^[24] The PDR images with the mandible may provide information about dental status, age range, and gender. It is also conceivable to perform identification of a dead body or living individual whose identity is unknown, with such limited data on hand. Many diverse manual techniques are employed for gender prediction from PDR images of teeth. For instance, while an adult's skull is a reference material to identify gender with an accuracy of 80%, this accuracy can rise to 90% when the mandible is taken into account, additionally.^[33] Although manual approaches are prone to error, the application of the aforementioned techniques requires a certain amount of time and experienced specialists (forensic anthropologist, pathologist, etc.) who are familiar with such techniques.^[34,35] As a result, the PDR images, acquired with fully automatic image techniques, covering the entire mandible and contributing positively to biometric identification; and thereby providing a holistic approach, were used for gender classification in our study.

It is possible to identify gender and age from skeletal remains in forensic medicine, osteology, and physical anthropology; however, gender determination by age is considered the most challenging issue.^[36] The process of manually separating morphological characters for gender classification is common. Due to the intricacy of PDR images, researchers mostly concentrate on different morphometric and non-metric parameters of the mandible.^[37,38] As a result of morphometric studies, Loth et al. achieved over 90% classification success as grounding on the characteristic of the ramus flexure, which is absent in males but is present in female individuals and is also regarded as a part of the mandible.^[39] Lin et al. set the upper limit of mandibular flexure, the maximum ramus vertical height, and upper ramus vertical height as discrimination parameters and correctly classified 81.7% to 88.8% gender classification among 240 three-dimensional mandibular models.^[25] In the cited manual studies in the literature, there were intact mandibles used without any pathology, loss of mandibular molars or abnormal molars, and teeth. Denis et al. proposed an automated solution for gender estimation based on deep learning techniques using convolutional neural networks from PDR images instead of employing only specific metric and non-metric indicators. However, as the test dataset advanced from 400 to 2000, the accuracy rate reduced from 96.8% to 92.3%.^[21] Ivan et al. used deep convolutional neural networks (DCNN), which have attested successfully in image analysis, and achieved 94.3% accuracy in the test dataset used in DCNN models.^[33] Based on the convolutional neural network developed by a multi-feature fusion module, Wenchi et al. suggested a new automated technique for gender estimation from panoramic dental x-ray images. With the method proposed, they attained 94.6% \pm 0.58% accuracy on the test dataset they used.^[40] Ortiz et al. propounded a new technique for gender estimation through anatomical points that appear on panoramic radiographs using machine learning techniques. The accuracy rate was 68% for women and 74% for men.^[41] The novel methods reported in the literature for gender estimation are mainly based on deep learning approaches and do not require any manual feature adjustment.

In addition to these studies, pre-processing techniques to improve the quality of dental images according to the recent past are presented in (Table 1), various studies in dentistry that consider deep learning-based techniques are presented in (Table 2).^[42]

Materials and Methods

Dataset collection and preparation

The study examined a dataset of 24,000 PDR images from patients aged between 18 and 77 who received dental treatment in Diyarbakir Oral and Dental Health Hospital Periodontology clinic between 2015 and 2020. The female and male patient ratio in the data set was 58% and 42%, respectively. The images were captured using the Planmeca Promax 2D digital panoramic x-ray machine (anodic voltage 50-84 KV, current 0.5-16 mA, Planmeca, Finland) available in the clinic. The acquired PDR pictures had considerable differences in terms of contrast, location, and resolution parameters. That variation was one of the factors complicating gender identification. (Figure 1) and (Figure 2) illustrates sample female and male PDR images taken from a variety of patients. The PDR images were pre-processed to reduce complexity and focus on the mandible area. The histogram equalization method was applied to interpret the mandible area and teeth.

Furthermore, the resolution of original PDR images was resized from 3180×1509 to 224×224 pixels for the deep learning model without interfering with the aspect ratio value. An Open CEZERI Library (OCL) was utilized for pre-processing.^[52]

(Table 3) lists the distribution of the PDR image dataset 64%, 16%, 20% as training, validation and test set, respectively. Additionally, (Figure 3) depicts the ranges of gender and age distribution. It is clear from the histogram graph that the number of patients aged between 25 and 50 are higher than the others.

Proposed model

DenseNet121^[53] architecture was used as a deep learning model in binary classification of PDR images. In addition, transfer learning technique was applied to increase the performance of the model.

DenseNet

Convolution in the training of the convolutional neural networks and increment in subsampling steps causes a decrease in feature maps. Also, gradient loss occurs in the image feature during transitions between cross-layers. The DenseNet architecture is designed to take advantage of feature maps more effectively and reduce vanishing gradient loss. A dense layer takes the output of all previous layer and merges it according to the depth dimension. Each dense block in the DenseNet architecture has two convolution layers (convolutions) of varying number of repetitions.^[53]

In the classical CNN architecture, while each layer only has information about the feature map received from the previous layer, in the DenseNet architecture, however, each layer is updated with the inputs of all back layers. Since each layer is coupled feed-forwardly to others, any layer can access the feature information of all preceding layers. Reutilization of the feature map in dense blocks by different layers boosts the input and performance of the next layer, allowing for the generation of easy-to-train models.

(Figure 4) shows the comparison of the classical CNN model with the DenseNet model. When analysing layer three in (Figure 4), the DenseNet model is comprehended to receive information from all back layers, whereas the CNN model only gets input from the preceding layer, which is layer two. Using such a strategy improves the flow of information and feature maps in the DenseNet, resulting in a minimum loss. Several variants have been designed that belongs to the DenseNet family including DenseNet121, DenseNet169, and DenseNet201.^[53]

When the feature coupling is mathematized; if X_0 is defined as the input image, then the H can be defined as a composite function consisting of three consecutive steps. In other words, H the transfer function, consists of a combination of BN, ReLU, and 3×3 convolution (conv.).

For the general CNN, while 'th output is generated by the $l - 1$ 'th input,

$$X_l = H_l(X_{l-1}) \quad (1)$$

In the DenseNet architecture, each layer concatenates the feature maps of previous layers and uses them as input for itself.

Thus, 'th output is used as X_0, \dots, X_{l-1} input via taking the feature maps of all preceding layers and defining them as their assembly.

$$X_l = H_l([X_0, X_1, X_2, \dots, X]) \quad (2)$$

In the DenseNet, the size of the feature map expands as it passes through each dense layer and compiles existing features (the k parameter) from previous layers. The

growing rate indicated by the parameter k defines how dense architecture produces the most advanced outcomes.

Thanks to the concatenate node built between the layers, the DenseNet performs well enough, despite having fewer parameters than the classical CNN architecture. The DenseNet121 model we proposed achieved better performance with approximately 7M parameters when compared to other models we tested in binary classification analysis. If every l 'th layer of H generates k unit of the feature map, then l 'th layer can be defined as:

$$k_l = k_0 + k \times (l-1) \quad (3)$$

Here, k_0 refers to the number of channels in the input layer.^[53]

(Figure 5) shows the functionality of the DenseNet121 workflow, which includes a combination of Dense Block and Transition Layer for gender classification of the PDR image given in the introduction. Each architecture in the DenseNet model has four dense blocks and three transition layers. Dense blocks each have layers called bottlenecks. 1×1 conv. reduces the number of channels in the input, 3×3 conv. performs the converted convolution of the input with the reduced channel number. Also, the (1×1 conv.) and (3×3 conv.) layers contain a rectified linear unit (ReLU) activation with a batch normalization (BN) layer. The transition layer performs two operations, convolution and pooling. To perform feature concatenation, feature maps must be of similar size in the dense block. The bottleneck convolution layer can be added before each convolution, reducing the number of input feature maps and thus improving overall computational performance. The transition layers of the DenseNet architecture have a BN layer and convolution layer that accompany the average pooling layer. After the last dense block, a global average pooling layer is followed by a fine-tuned neural network block which is then fed to a Softmax classifier.^[53,54] The newly added block defines the combination of features required for new training examples, while saving computational complexity and time. It increases the representative learning of the modified model with the help of fine tuning on our dataset.

Transfer learning

Transfer Learning is a deep learning method in which model parameters are used on a large pre-trained dataset. In other words, transfer learning is a method of machine learning where we reuse a previously trained model as a starting point for a model in a new task. Model normalization is performed on the ImageNet dataset. ImageNet^[55] is one of the known datasets for training high-level neural networks. It contains more than 1.2 million images divided into 10,000 categories. Transfer learning is used in problems where there is not enough data for training or we want better results in a short time.

Fine tuning

Learning transfer is divided into different groups according to source/target learning, training and data. In our proposed deep learning model, high-level features in CNN had no effect, as the target dataset is small and different from the source dataset. The last layer was removed from the pre-trained model and new fully connected layer networks were added, taking into account the number of classes in the target data set. The weights in the trained CNN network are kept constant by assigning random values to the weights of the new fully connected layers.

DenseNet121# model

To develop the DenseNet121, we start with a pre-trained CNN model on the ImageNet dataset. We expand and fine-tune the network with a few additional layers before the final layer to increase the ability to understand more complex patterns from the data. At the end of this fine-tuning phase, we train on the dental dataset related to our target task, which includes PDR images, making it more experienced. We defined our proposed model from the combination of DenseNet121#, Fine tuning & Transfer learning & DenseNet121. (Figure 6) shows an overview of the model approach. To compare the performance of our proposed model, a dataset was created from image and tag pairs trained on a similar architecture to VGG, ResNet, EfficientNet deep transfer models. In our study, a 5-fold cross-validation technique was used to avoid overfitting or bias and to evaluate model training.^[56] The 19,200 PDR images selected as the training dataset were randomly divided into five layers, and the dataset of each layer was sliced into 80 to 20 percent slices. The model was established using the train set in all steps and evaluated with the validation set. The statistical summary of the evaluation scores of the model was examined. An overview of the 5-fold cross validation performed in this study is presented in (Figure 7). This process was repeated for each architecture (VGG16, ResNet50, EfficientNetB6 and DenseNet121#) and the averages found as a result of the trials were reflected in the tables.

The adjusted hyper-parameters of our model consist of the learning rate, batch size, dropout rate, number of epochs, and optimizer. (Table 4) lists the hyper-parameters used to train the proposed deep transfer model. In the performance analysis, the best accuracy rate with the minimum loss was attained using the values provided in (Table 4). The Adam optimizer algorithm was used to optimize several DCNN models containing medical images.^[57] In addition, when compared to other optimizers such as Stochastic Gradient Descent (SGD) and RMSProp, the Adam optimizer had an appropriate function with minimal memory consumption and fast convergence.^[58] Our test dataset are approximately 4,800 PDRs, and such an amount could be regarded within the range of an adequate number to evaluate the performance of a gender estimation.

Evaluation metrics

The confusion matrix is one of the most significant performance criteria in multi-classification problems. In this context, the accuracy, sensitivity, specificity, recall, and F1 score criteria are calculated through the confusion matrix.^[59]

The confusion matrix expresses the accuracy of the classifier by comparing the actual and predicted label values. (Table 5) shows the general structure of a confusion matrix. True positive (TP) and true negative (TN) are where the model predicts the correct answer; false positive (FP) and false negative (FN) are where the model gets it wrong.

The accuracy refers to the ratio of correct (true) data defined to all data used. It is calculated as follows.^[59]

$$\text{accuracy} = \frac{(\text{TP} + \text{TN})}{(\text{TP} + \text{TN} + \text{FP} + \text{FN})} \quad (4)$$

The precision refers to the ratio of positive data identified as true to all data identified as true. It is calculated as follows.^[60]

$$\text{precision} = \frac{(\text{TP})}{(\text{TP} + \text{FP})} \quad (5)$$

The specificity refers to the ratio of negative data defined as true to the sum of negative data defined as true and positive data defined as false. It is calculated as follows.^[60]

$$\text{specificity} = \frac{(\text{TN})}{(\text{TN} + \text{FP})}$$

(6)

The recall refers to the ratio of positive data identified as true to the sum of positive data identified as true and negative data identified as false. It is calculated as follows.^[61]

$$\text{recall} = \frac{(\text{TP})}{(\text{TP} + \text{FN})}$$

(7)

F_Score is calculated as the harmonic mean of sensitivity and recall, and it has a better measurement than the accuracy.^[60]

$$F_{\text{score}} = 2 \times \frac{(\text{precision}) \times (\text{recall})}{(\text{precision}) + (\text{recall})}$$

(8)

The processing steps required for gender classification from PDR images are summarized in (Figure 8).

Experimental Results

In this study, biological gender prediction was made from PDR images using DenseNet deep learning model. Initially, experimental analyses were made for DenseNet architectures (121-169-201), and DenseNet121# architecture came to the fore with the highest accuracy value among the architectures. When the analysed architectures were compared, DenseNet121# architecture was chosen as the reference model in terms of the number of parameters and performance criteria. Test accuracy values for DenseNet architectures (121-169-201) are given in (Table 6).

The test accuracy values of the proposed DenseNet121# architecture for different image resolutions are given in (Table 7). It has been observed that the accuracy value of the 96×96 resolution PDR images is lower than the 224×224 resolution.

(Table 8) shows the performance accuracy values the four transfer learning models compared. The selected hyper-parameters were employed in the training of four deep transfer learning. It was noteworthy that the accuracy value of the VGG16 was dramatically low. DenseNet121# architecture was observed to have the highest accuracy value among other architectures. The test inference times of the model architectures used are shown in (Figure 9).

The confusion matrix is used to find the minimal false-negative and false-positive result values. Confusion matrix was used to describe the performance of the DenseNet121 architecture on the separated test data. The confusion matrix defining the effect of false-positive and false-negative rates is shown in (Figure 10). Also the confusion matrix summary for the deep learning models used is given in (Table 9). The referenced DenseNet121# architecture correctly classified 97.25% of the samples.

While estimating gender from PDR images, the Gradient-weighted Class Activation Mapping (Grad-CAM) method reported in^[62] was used to identify the areas to focus on in the identification process. The matrix produced by the filters in the last CNN layer of the DenseNet121# architecture is superimposed on the actual PDR image for

this purpose. The visualization of the feature map superimposed on the female and male PDR test images is shown in (Figure 11). The CNN feature map concentrating on the focus area is shown in the initial columns in (Figure 11). The colors in the feature map refer to the convolutional neural network's targeted areas. The network's focus gradually increases as the color shifts from yellow to red. However, the secondary columns represent a coupling condition (high similarity score). The overlaid map in this column shows the focused areas with brighter yellowish and reddish colors spread over a wider area covering the maxillary, mandibular, and nasal sections. Considering the Grad-CAM and superimposed images examined, the proposed model is acknowledged to focus on the mandible and the teeth area and is a suitable and reliable instrument for forensic medicine practices.

(Figure 12) and (Figure 13) shows the performance graph of the training/test accuracies and losses of the DenseNet121 architecture for the 19,200 sampled training dataset. It was observed that the proposed model attained significant accuracy and loss values even in the 50th epoch.

A summary of studies for gender estimation from PDR images is given in (Table 10). Since the codes and data sets of the studies on gender classification could not be reached from the PDR images available in the literature, a completely fair and rational comparison could not be made between the previous studies and the study we proposed.

Conclusion

In this study, we proposed the DenseNet121# architecture of the DenseNet model, which uses a deep transfer learning network and a fully automated technique to process panoramic dental x-ray images. The structural flexibility and have fewer parameters of the DenseNet121# architecture contributed to the increase in performance by accelerating the training and validation processes. A combination of weighted loss function and transfer learning was used to eliminate the imbalance in gender classification. The best performance was achieved for the 4,800 test datasets with a classification accuracy of 97.25%. The proposed model, along with Grad-CAM-based analysis, also revealed that the most important areas to consider in gender classification were the mandible and teeth.

In conclusion, this study focused on the gender classification problem as it forms an important part of PDR image interpretation in both dental biometric information-based human identification systems and clinical dentistry.

Conflict of interest

There are no conflicts of interest.

Financial Support

None.

References

1. Ataş M, Ayhan T. Development of Automatic Tree Counting Software from UAV Based Aerial Images with Machine Learning. CoRR, v. abs/2201.02698, 2022.

2. Doğan Y, Ataş M. Prediction of adaptive exposure time in hyperspectral bands for industrial cameras. 23rd Signal Processing and Communications Applications Conference (SIU)-IEEE 2015.
3. Ozdemir C, Gedik MA, Kaya Y. Age Estimation from Left-Hand Radiographs with Deep Learning Methods. *Traitement du Signal*. 2021;38:1565-74.
4. Ataş M, Yeşilnacar Mİ, Yetiş AD. Novel machine learning techniques based hybrid models (LR-KNN-ANN and SVM) in prediction of dental fluorosis in groundwater. *Environmental Geochemistry and Health* 2021. pp. 1-15.
5. Ulah A, Şahin CB, Dinler OB, Khan MH. Heart Disease Prediction Using Various Machines Learning Approach. *Journal of Cardiovascular Disease Research* 2021;12:379-91.
6. Ataş M, Özdemir C, Ataş İ, Ak B, Özeroğlu E. Biometric identification using panoramic dental radiographic images with few-shot learning. *Turk J Elec Eng & Comp Sci* 2022;30:1115-26.
7. Dogan Y, Atas M, Özdemir C. A new approach for plotting raster based image files. 22nd Signal Processing and Communications Applications Conference (SIU)-IEEE 2014.
8. Ataş M, Doğan Y, Ataş İ. Fast Weighing of Pistachio Nuts by Vibration Sensor Array. *International Journal of Electronics and Electrical Engineering* 2016; 4:313-17.
9. Ataş M, Ataş İ. Prediction of Resonance Frequency of Aperture Coupled Microstrip Antennas by Artificial Neural Network. *International Journal of Engineering Sciences & Research Technology* 2016;5:252-60.
10. Özdemir C, Ataş M, Özer AB. Classification of Turkish spam e-mails with artificial immune system. 21st Signal Processing and Communications Applications Conference (SIU)-IEEE 2013.
11. Dinler ÖB, Aydın N. An optimal feature parameter set based on gated recurrent unit recurrent neural networks for speech segment detection. *Applied Sciences* 2020;10:1273-96.
12. Özdemir C, Ataş M. A novel similarity algorithm for fixing erroneous Turkish text and detection of roots. 22nd Signal Processing and Communications Applications Conference (SIU)-IEEE 2014.
13. Dinler ÖB, Şahin CB. Prediction of phishing web sites with deep learning using WEKA environment. *Avrupa Bilim ve Teknoloji Dergisi* 2021;24:35-41.
14. Ataş M. Hand tremor based biometric recognition using leap motion device. *IEEE Access* 2017;5:23320-26.
15. Şahin CB, Dinler ÖB, Abualigah L. Prediction of software vulnerability based deep symbiotic genetic algorithms: Phenotyping of dominant-features. *Applied Intelligence* 2021;51:8271-87.
16. Dogan Y, Keles HY. Semi-supervised image attribute editing using generative adversarial networks. *Neurocomputing* 2020;401:338-52.
17. Dogan Y, Keles HY. Iterative facial image inpainting based on an encoder-generator architecture. *Neural Comput & Application* 2022;34:10001–21.
18. Ataş M, Yardimci Y, Temizel A. A new approach to aflatoxin detection in chili pepper by machine vision. *Computers and electronics in agriculture* 2012;87:129-41.
19. Yetis AD, Yesilnacar MI, Atas M. A machine learning approach to dental fluorosis classification. *Arabian Journal of Geosciences* 2021;14:1-12.
20. Ataş M, Tekeli AE, Dönmez S, Fouli H. Use of interactive multisensor snow and ice mapping system snow cover maps (IMS) and artificial neural networks

- for simulating river discharges in Eastern Turkey. *Arabian Journal of Geosciences* 2016;9:1-17.
21. Denis M, Marin V, Ivan G, Marko S. Estimating Biological Gender from Panoramic Dental X-Ray Images. 11th International Symposium on Image and Signal Processing and Analysis (ISPA) 2019.
 22. Sweet D. INTERPOL DVI best-practice standards-An overview. *Forensic Science International* 2010. pp. 18–21.
 23. Jardin P, Ponsaillé J, Alunni-Perret V, Quatrehomme G. A comparison between neural network and other metric methods to determine sex from the upper femur in a modern French population. *Forensic Sci. Int* 2009;192:121-26.
 24. Badran DH, Othman DA, Thnaibat HW, Amin WM. Predictive Accuracy of Mandibular Ramus Flexure as a Morphologic Indicator of Sex Dimorphism in Jordanians. *Int. J. Morphol* 2015;33:1248-54.
 25. Lin C, *et al.* Sex determination from the mandibular ramus flexure of Koreans by discrimination function analysis using three-dimensional mandible models. *Forensic Sci. Int.* 2014;236:191-96.
 26. Kim DI, Kim YS, Lee UY, Han SH. Sex determination from calcaneus in Korean using discriminant analysis. *Forensic Sci. Int.* 2013;228:171-77.
 27. Mahfouz M, *et al.* Patella sex determination by 3D statistical shape models and nonlinear classifiers. *Forensic Sci. Int.* 2007;173:161–70.
 28. Gapert R, Black S, Last J. Sex determination from the occipital condyle: Discriminant function analysis in an eighteenth and nineteenth century British sample *Am. J. Phys. Anthropol.* 2009;138:384-94.
 29. El Morsi DA, Al Hawary AA. Sex determination by the length of metacarpals and phalanges: X-ray study on Egyptian population. *J. Forensic Leg. Med.* 2013;20:6–13.
 30. Oner Z, Turan MK, Oner S, Secgin Y, Sahin B. Sex estimation using sternum part lengths by means of artificial neural networks. *Forensic Sci. Int.* 2019;301:6–11.
 31. [Toy S](#), *et al.* A study on sex estimation by using machine learning algorithms with parameters obtained from computerized tomography images of the cranium. *Nature* 2022;12:4278-89.
 32. Hu KS, *et al.* Sex determination using nonmetric characteristics of the mandible in Koreans. *Journal of forensic* 2006;51:1376–82.
 33. Ivan I, Marin V, Marko S. Gender Estimation from Panoramic Dental X-ray Images using Deep Convolutional Networks. 2019.
 34. Lai Y, *et al.* LCANet: Learnable Connected Attention Network for Human Identification Using Dental Images. *IEEE Transactions on Medical Imaging* 2021;40:905-15.
 35. Chen H, Jain AK. Tooth contour extraction for matching dental radiographs. 17th International Conference on Pattern Recognition; Cambridge 2004. pp. 522–25.
 36. Balci Y, Yavuz MF, Cagdir S. Predictive accuracy of sexing the mandible by ramus flexure. *Homo.* 2005;55:229-37.
 37. Oliveira GT, Alves MC, Haiter NF. Mandibular sexual dimorphism analysis in CBCT scans. *Journal of Forensic and Legal Medicine* 2016;38:106–10.
 38. Maloth KN, *et al.* Mandibular ramus: A predictor for sex determination-A digital radiographic study. *Journal of Indian Academy of Oral Medicine and Radiology* 2017;29:242-46.

39. Loth SR, Henneberg M. Mandibular ramus flexure is a good indicator of sexual dimorphism. *Am. J. Phys. Anthropol.* 1998;105:91-92.
40. Wenchi K, *et al.* Biological Gender Estimation from Panoramic Dental X-ray Images Based on Multiple Feature Fusion Model. *Sensing and Imaging* 2020, pp. 54.
41. Ortiz AG, Costa C, Silva RHA, Biazevic MGH, Michel-Crosato E. Sex estimation: Anatomical references on panoramic radiographs using Machine Learning. *Forensic Imaging* 2020;20:200-356.
42. Kumar A, Bhadauria HS, Singh A. Descriptive analysis of dental X-ray images using various practical methods: A review. *PeerJ Computer Science* 2021.
43. Zak J, *et al.* The method of teeth region detection in panoramic dental radiographs. *International Conference on Computer Recognition Systems* 2017, pp. 298–307.
44. Mahdi FP, Kobashi S. Quantum particle swarm optimization for multilevel thresholding-based image segmentation on dental x-ray images. *Joint 10th International Conference on Soft Computing and Intelligent Systems (SCIS) and 19th International Symposium on Advanced Intelligent Systems (ISIS)* 2018, pp. 1148–53.
45. Fariza A, Arifin AZ, Astuti ER, Kurita T. Segmenting tooth components in dental x-ray images using Gaussian kernel-based conditional spatial Fuzzy C-Means clustering algorithm. *International Journal of Intelligent Engineering and Systems* 2019;12:108–17.
46. Aliaga I, *et al.* Automatic computation of mandibular indices in dental panoramic radiographs for early osteoporosis detection. *Artificial Intelligence in Medicine* 2020, 101816.
47. Rasool EPD. Sex classification of first molar teeth in cone beam computed tomography images using data mining. *Forensic science international* 2020, 110633.
48. Oktay AB. Tooth detection with convolutional neural networks. *Medical Technologies National Congress* 2017, pp. 1–4.
49. Chu P, *et al.* Using octuplet siamese network for osteoporosis analysis on dental panoramic radiographs. *40th Annual International Conference of the IEEE Engineering in Medicine and Biology Society (EMBC)* 2018, pp. 2579–82.
50. Lee JH, Han SS, Kim YH, Lee C, Kim I. Application of a fully deep convolutional neural network to the automation of tooth segmentation on panoramic radiographs. *Oral Surgery, Oral Medicine, Oral Pathology and Oral Radiology* 2019;129:635–42.
51. Muramatsu C, *et al.* Tooth detection and classification on panoramic radiographs for automatic dental chart filing: improved classification by multi-sized input data. *Oral Radiology* 2020, pp. 1–7.
52. Ataş M. Open Cezeri Library: A novel java based matrix and computer vision framework. *Computer Applications in Engineering Education* 2016;24:736-43.
53. Huang G, Liu Z, Van Der Maaten L, Weinberger KQ. Densely connected convolutional networks. *Proceedings of the IEEE Conference on Computer Vision and Pattern Recognition* 2017, pp. 4700–08.
54. Tavishee C, Hemant P, Sarveshmani T. Optimization and fine-tuning of DenseNet model for classification of COVID-19 cases in medical imaging. *International Journal of Information Management Data Insights* 2021, pp. 100020.

55. Deng J, *et al.* ImageNet: A large-scale hierarchical image database. in Proc. IEEE Conf. Comput. Vis. Pattern Recognit. 2009, pp. 248–255.
56. Stone M. Cross-validatory choice and assessment of statistical predictions. *J. R. Stat. Soc. Ser. B Methodol* 1974;36:111–33.
57. Kandel I, Castelli M, Popovic A. Comparative study of first order optimizers for image classification using convolutional neural networks on histopathology images. *J. Imaging* 2020;6:92.
58. Kingma DP, Ba J. Adam: A Method for Stochastic Optimization. *CoRR*, v. abs/1412.6980, 2017.
59. Sokolova M, Japkowicz N, Szpakowicz S. Beyond accuracy, Fscore and ROC: A family of discriminant measures for performance evaluation. In *Australasian Joint Conference on Artificial Intelligence 2006*, pp. 1015–1021.
60. Marin I, Mladenovic S, Gotovac S, Zaharija G. Deep-Feature-Based Approach to Marine Debris Classification. *Applied Sciences* 2021;11:5644-69.
61. Liu C, White M, Newell G. Measuring and comparing the accuracy of species distribution models with presence–absence data. *Ecography* 2011;34:232–43.
62. Selvaraju RR, *et al.* Grad-CAM: visual explanations from deep networks via gradient-based localization. In: *IEEE International Conference on Computer Vision; Venice 2017*, pp. 618–26.
63. Nagaraj LJ, Gogula S, Ghouse N, Nigam H, and Sumana CK. Sex determination by using mandibular ramus: A digital radiographic study. *Journal of Medicine, Radiology, Pathology and Surgery* 2017;4:5–8.
64. [Alias A](#), [Ibrahim A](#), [Abu Bakar ST](#). Anthropometric analysis of mandible: an important step for sex determination. *The National Center for Biotechnology Information advances science and health by providing access to biomedical and genomic information* 2018;169:217-23.
65. Mualla N, Houssein E, Hassan MR. Dental Age Estimation Based on X-ray Images. *CMC-Computers, Materials & Continua* 2020;62:591-605.
66. Rajee MV, [Mythilib C](#). Gender classification on digital dental x-ray images using deep convolutional neural network. [Biomedical Signal Processing and Control](#) 2021;69:102939.
67. Santosh KC, Nijalingappa P, Vikas G, Raju R, Ekta P, Piyush KS, Stephen JN. Machine Learning Techniques for Human Age and Gender Identification Based on Teeth X-Ray Images. *Advances in Feature Transformation based Medical Decision Support Systems for Health Informatics 2022*, pages:14.

Table 1: Pre-processing techniques are addressed to recuperate the quality of dental images by year

Year	Relevant review finding	Detection/ Identification
2017 ^[43]	Individual arc teeth segmentation (IATS) with adaptive thresholding is applied to find the palatal bone.	Teeth detection
2018 ^[44]	Quantum Particle Swarm Optimization (QPSO) is employed for multilevel thresholding.	Teeth detection
2019 ^[45]	For tooth segmentation, the Gaussian kernel-based conditional spatial fuzzy c-means (GK-csFCM) clustering algorithm is used.	Teeth detection
2020 ^[46]	The region of interest is extracted from the entire X-ray image, and segmentation is performed using k-means clustering	Mandible detection
2021 ^[47]	Naive Bayesian (NB), Random Forest (RF) and Support Vector Machine (SVM) are used as classifiers for prediction.	Teeth detection

Table 2: Presents various studies considering deep learning-based techniques in the field of dentistry

Year	Deep learning architecture	Detection/ Application	Metric
2017 ^[48]	AlexNet	Teeth detection and classification	Accuracy
2018 ^[49]	Deep octuplet Siamese network (OSN)	Osteoporosis analysis	Accuracy
2019 ^[50]	Mask R-CNN model	Teeth segmentation for diagnosis and forensic identification	F1 score
2020 ^[51]	CNN (ResNet50)	Teeth detection and classification	Confusion Matrix
2021 ^[47]	Support Vector Machine (SVM)	Teeth detection and classification	Accuracy

Table 3: Training, validation and testing rates by gender in the PDR image dataset

Class Label	Train (64%)	Validation (16%)	Test (20%)	Total (100%)
Female	8,960	2,240	2,800	14,000
Male	6,400	1,600	2,000	10,000
Total	15,360	3,840	4,800	24,000

Table 4: Selected hyper-parameters to train the proposed deep transfer model

Hyper-parameters	Options
Learning rate	0.0001
Batch size	16
Dropout rate	0.5
Epochs	50
Optimizer	Adam

Table 5: Confusion matrix

Binary Classification	Predicted Positive (1)	Predicted Negative (0)
Actual Positive (1)	True Positive (TP)	False Negative (FN)
Actual Negative (0)	False Positive (FP)	True Negative (TN)

Table 6: Comparison of DenseNet architectures for test accuracy values

Model	Total Parameter	Accuracy
DenseNet121#	8M	0.9725
DenseNet169	14M	0.9345
DenseNet201	20M	0.9467

Table 7: Comparison of the proposed model architecture's accuracy at different image resolutions

Model	Resolution of PDR	Accuracy
DenseNet121#	96 × 96	0.8734
DenseNet121#	128 × 128	0.9233
DenseNet121#	224 × 224	0.9725

Table 8: Comparison of deep transfer learning model architectures

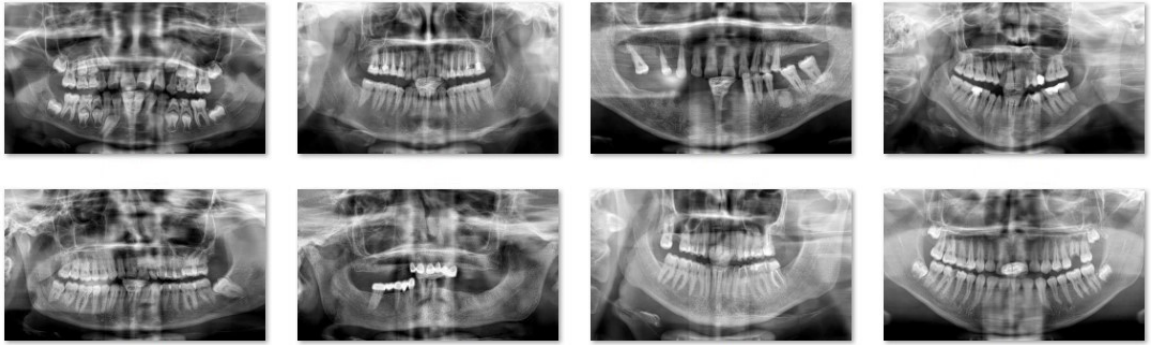
Architecture	Input Shape	Total Parameter	Accuracy
VGG16	(224, 224, 3)	15M	0.8220
ResNet50	(224, 224, 3)	26M	0.9260
EfficientNetB6	(224, 224, 3)	43M	0.9400
DenseNet121#	(224, 224, 3)	8M	0.9725

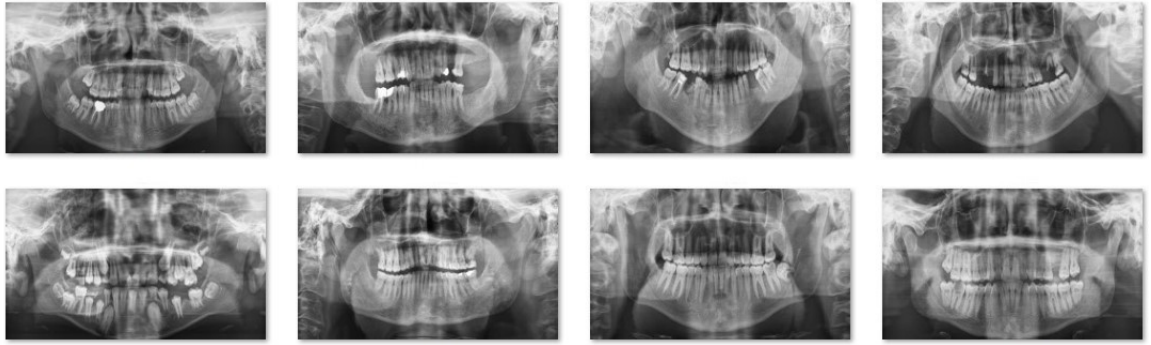
Table 9: Testing analysis of the proposed and the other deep learning based PDR classification model architectures

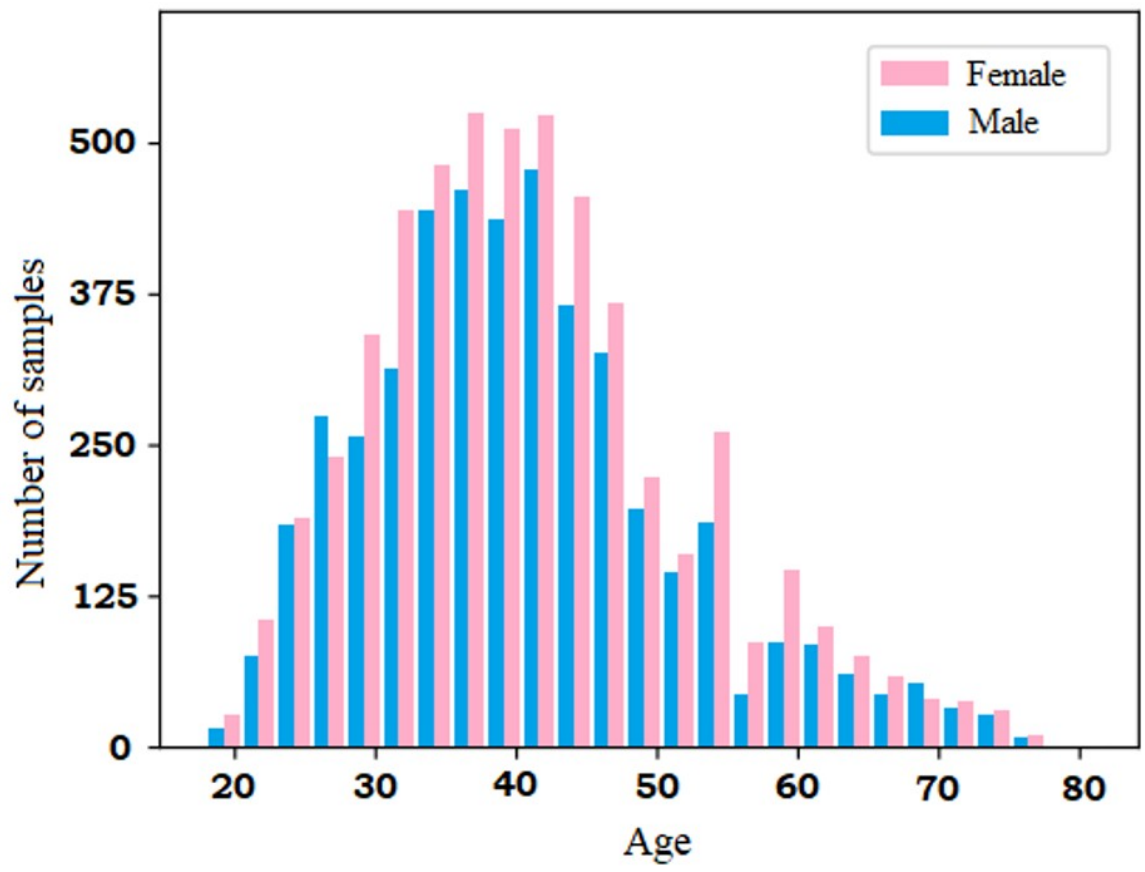
Model	VGG 16	ResNet 50	EfficientNet B6	DenseNet 121#
precision	0.8075	0.8958	0.9355	0.9680
recall	0.8262	0.9547	0.9447	0.9769
F1 Score	0.8219	0.9148	0.9390	0.9725
specifity	0.8175	0.9074	0.9355	0.9680
accuracy	0.8220	0.9260	0.9400	0.9725

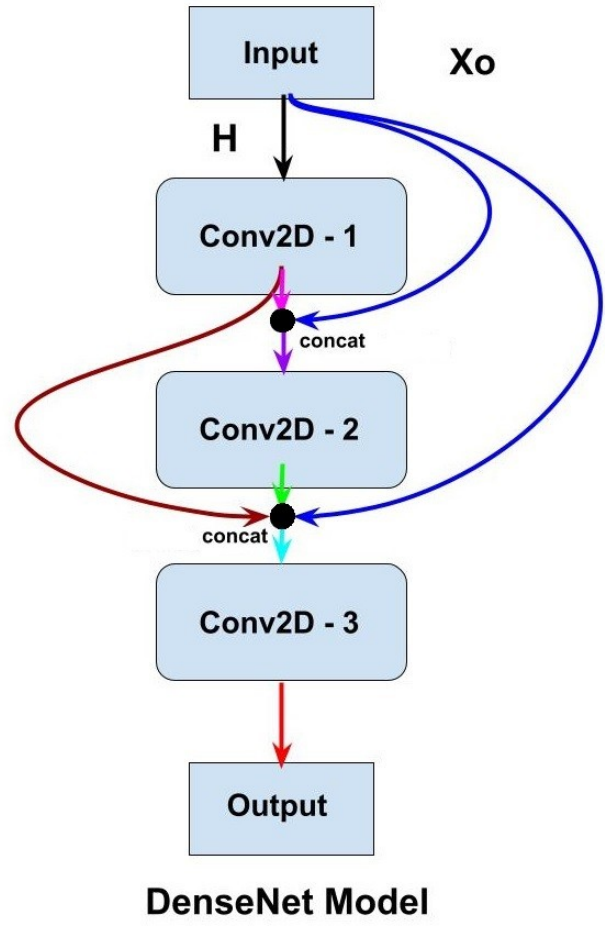
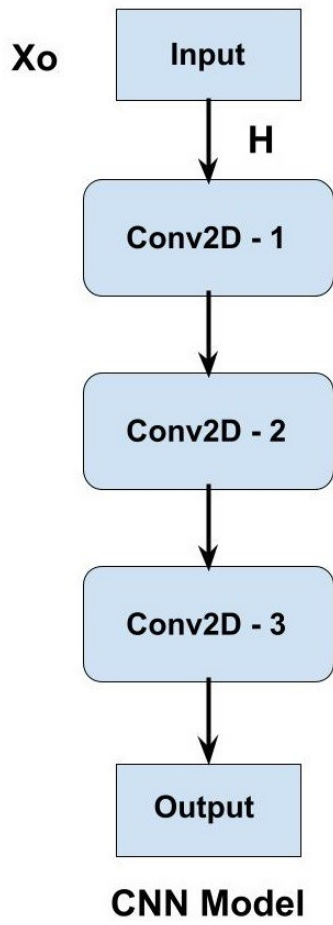
Table 10: Summary of studies for gender estimation from PDR images

Author	Years	Total Dataset	Dental Imaging Methods	Accuracy
Badran ^[24]	2015	419	Metric measurements	70.90%
Oliveira ^[37]	2016	160	Metric measurements	93.33 - 94.74%
Nagaraj ^[63]	2017	100	Metric measurements	71.00%
Alias ^[64]	2018	79	Metric measurements	78.50%
Denis ^[21]	2019	4,000	Convolutional Neural Network	96.87% ± 0.96%
Ivan ^[33]	2019	4,155	Deep Convolutional Network	94.30%
Wenchi ^[40]	2020	19,776	Multiple Feature Fusion	94.60% ± 0.58%
Mualla ^[65]	2020	1,429	Deep Neural Network	95.80%
Rajee ^[66]	2021	1,000	Deep Convolutional Neural Network	98.27%
Rasool ^[47]	2021	485	Support Vector Machine	92.31%
Santos ^[67]	2022	1,142	Library Support Vector Machine	96%
This study	2022	24,000	Deep Convolutional Neural Network	97.25%



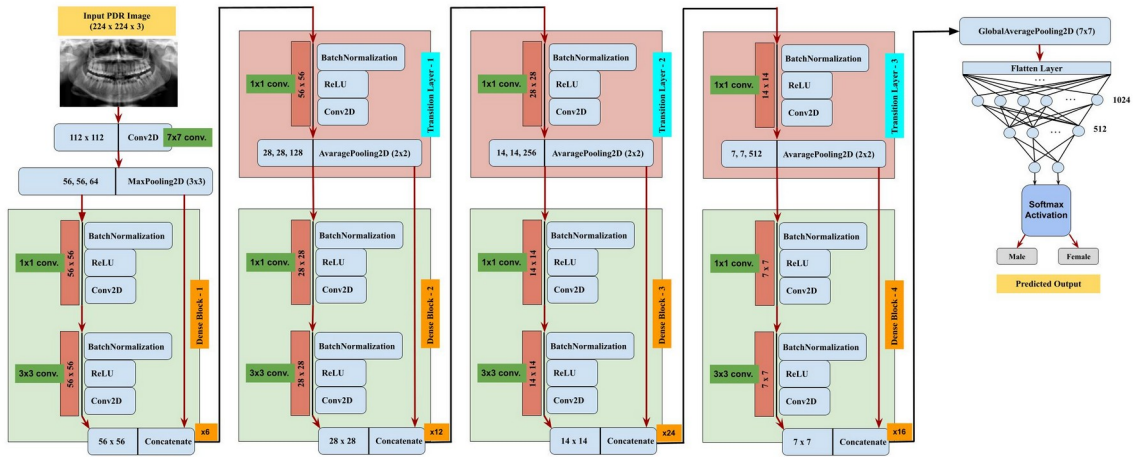


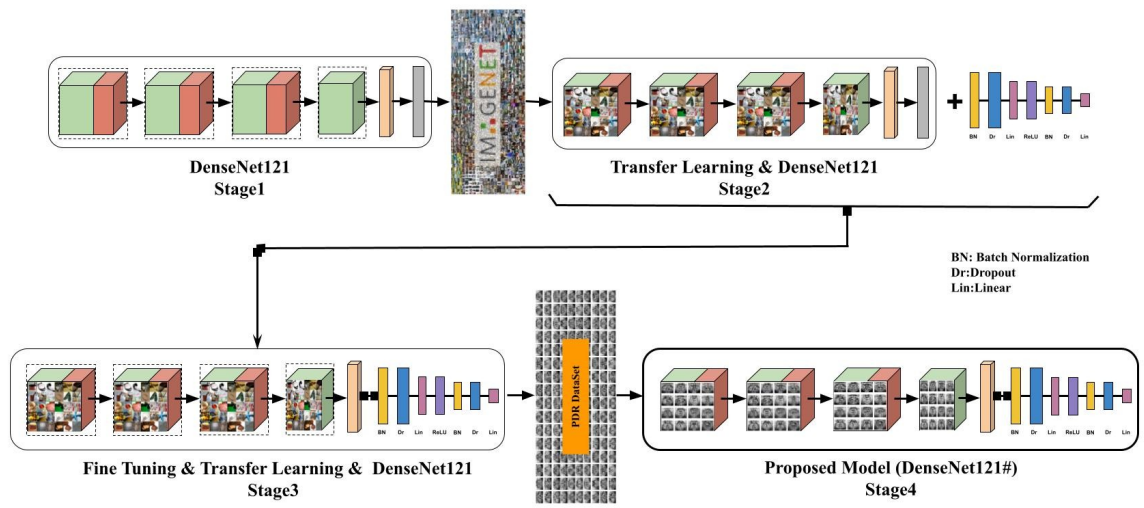


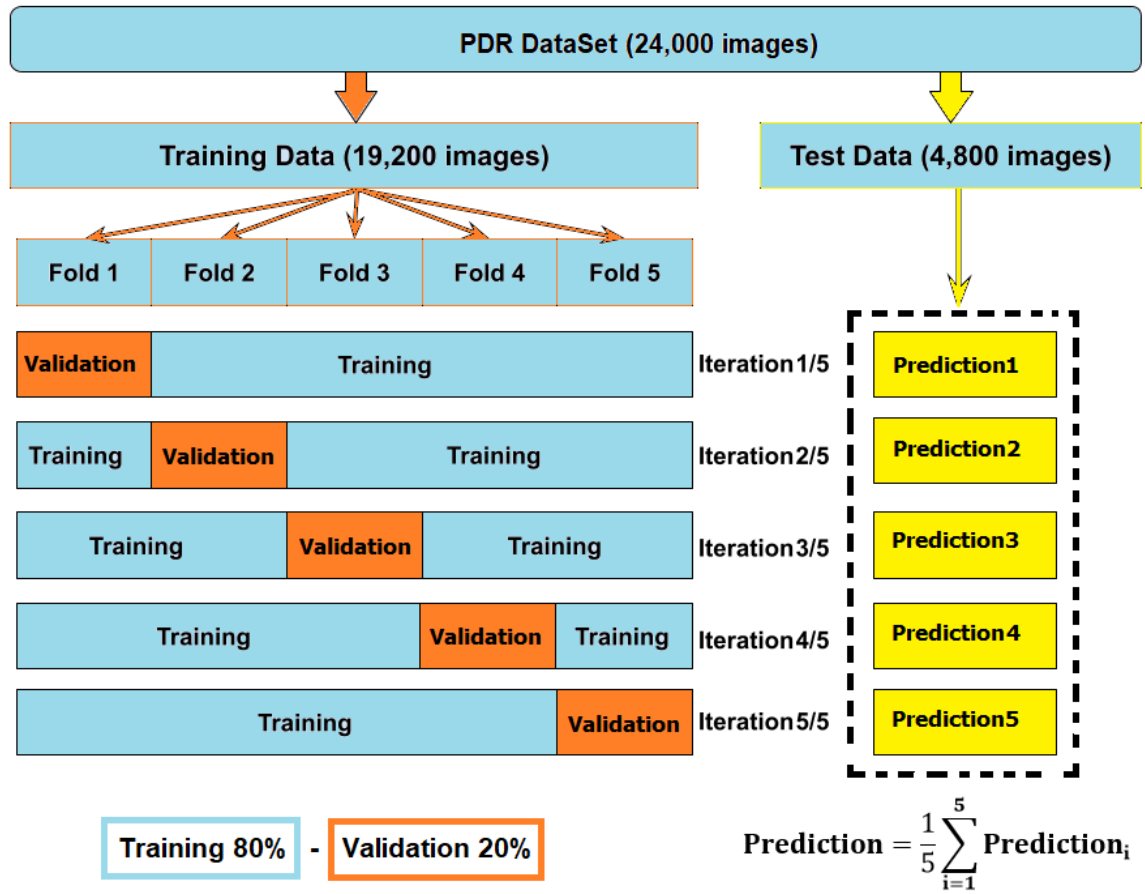


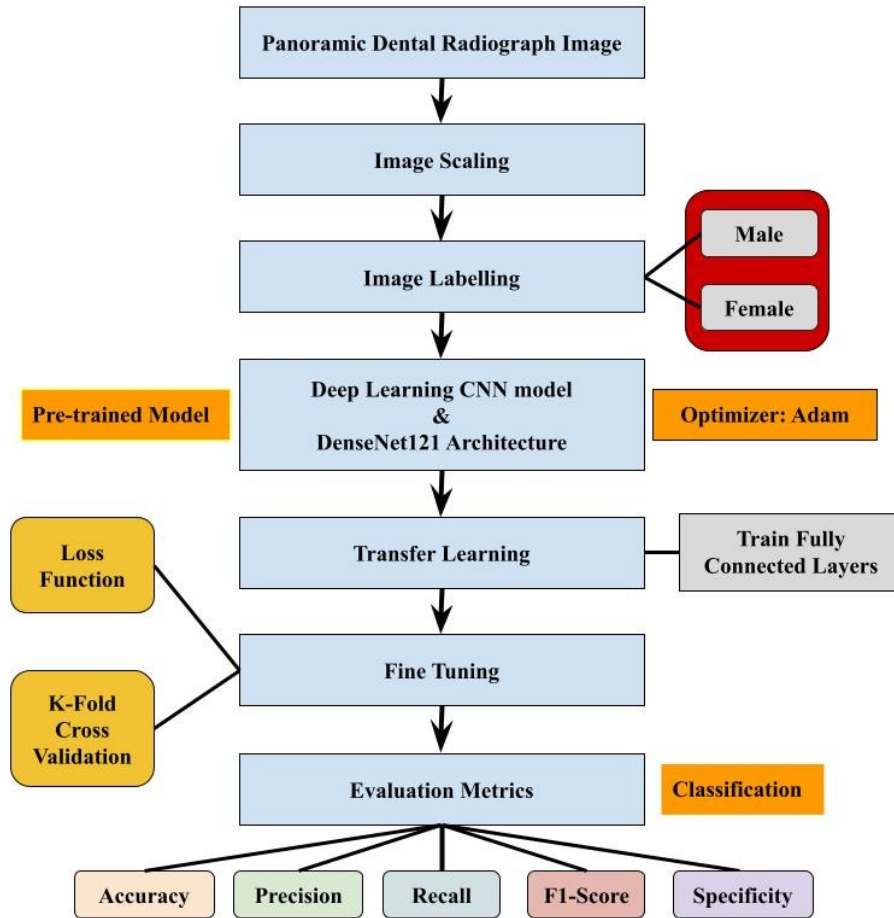
Transfer Learning - Feature Extraction (Pre-Trained Model)

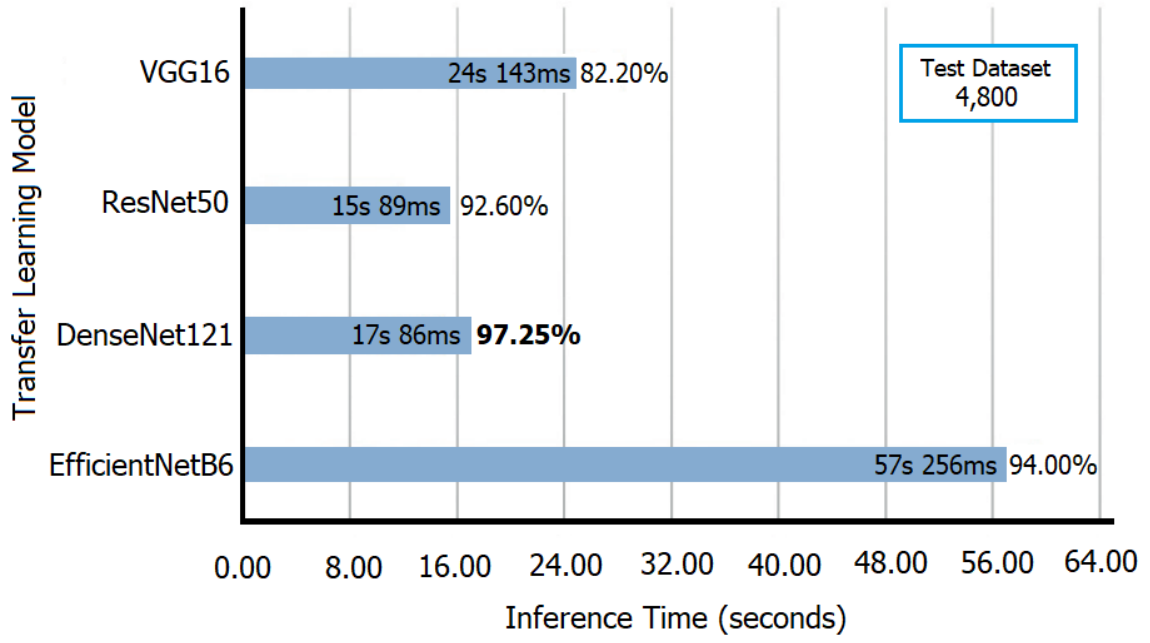
Classification (Fine-Tune Model)



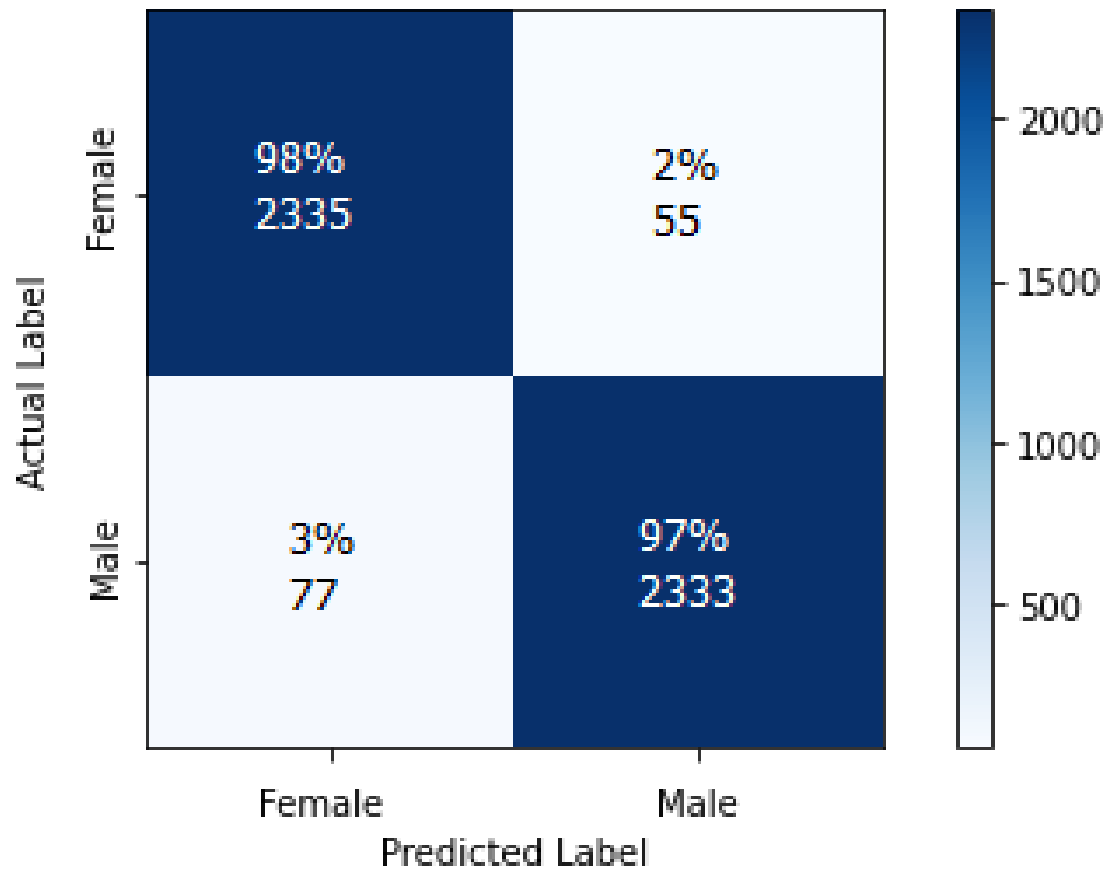


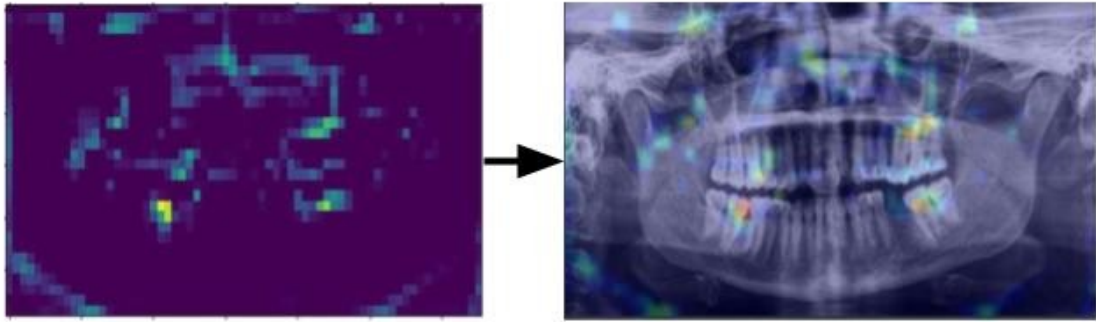






Confusion Matrix

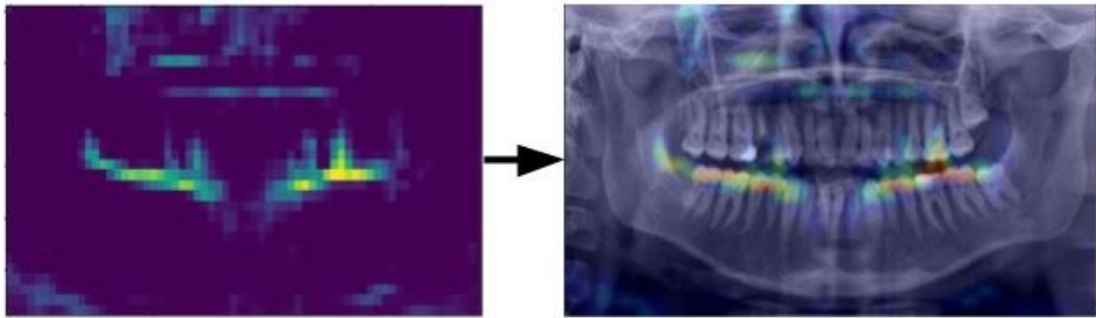




Grad-CAM (female)

(a)

Superimposed (female)



Grad-CAM (male)

(b)

Superimposed (male)

